Nanoparticle Size Effects on Methanol Electrochemical Oxidation on Carbon Supported Platinum Catalysts

Kleber Bergamaski, Alexei L. N. Pinheiro, Erico Teixeira-Neto, and Francisco C. Nart*

Instituto de Química de São Carlos, Universidade de São Paulo—C.P. 780—13566-590—São Carlos SP, Brazil

Received: May 30, 2006; In Final Form: August 4, 2006

The particle size effect observed on the performance of Pt/C electrocatalysts toward the methanol oxidation reaction (MOR) has been investigated with differential electrochemical mass spectrometry (DEMS). The investigation has been conducted under both potentiodynamic and potentiostatic conditions as research on methanol electrochemical oxidation is closely related to interest in direct methanol fuel cells. The particle size effect observed on the MOR is commonly regarded as a reflection of different Pt−CO and Pt−OH bond strengths for different particle sizes. This work focuses mainly on the mechanism of methanol dehydrogenation on platinum which is central to the problem of the optimization of the efficiency of methanol electro-oxidation by favoring the CO_2 formation pathway. It was found that the partitioning of the methanol precursor among the end products on supported platinum nanoparticles is strongly dependent on particle size distribution. Also, it is postulated that the coupling among particles of different sizes via soluble products must be considered in order to understand the particle size effects on the observed trends of product formation. An optimum particle size range for efficiently electro-oxidizing methanol to CO_2 was found between 3 and 10 nm, and loss in efficiency is mostly related to the partial oxidation of methanol to formaldehyde on either too small or too large particles. The possible reasons for these observations are also discussed.

Introduction

The intense research activity on methanol electrochemical oxidation is connected to interest in direct methanol fuel cells. There are many interesting reviews on the electrochemistry of methanol.[1−3] However, despite the large number of papers dedicated to this subject, there are still many open questions related to the mechanism of methanol electrochemical oxidation and its reactivity on fuel cell anodes.

The main products of methanol electro-oxidation on platinum have been identified as carbon dioxide, formaldehyde, and formic acid. The latter reacts with methanol to form methylformate, which allows the use of this species to follow the formic acid yield with DEMS.[4−6] Significantly, this reaction is more likely to occur in the solution phase rather than at the catalyst surface.[7] The route leading to the formation of CO_2 has the highest current efficiency, as the overall reaction involves 6 electrons. This reaction pathway is mediated by the formation of adsorbed carbon monoxide; thus, a high overpotential is required to oxidize this intermediate in order to complete the CO_2 pathway. On this account, the electro-oxidation of CO on platinum bimetallic catalysts has been the subject of many articles in the literature.[8] The adsorbed CO intermediate eventually takes over the metal surface as a poison at low overpotentials, utterly halting the methanol electro-oxidation via any route in the case of smooth platinum. This indicates that the remaining routes are also mediated by some adsorbed species. The pursuit of CO tolerant catalysts has drawn the efforts in the field of electrocatalysis mainly toward platinum alloys with oxophilic metals.[9] Nanoparticle platinum alloys have shown superior enhancement in the electro-catalytic activity toward the oxidation of small organic molecules, but the complexity of this system makes difficult the detailed exploration of the mechanism of methanol oxidation.

The routes bypassing adsorbed CO formation lead to soluble products (formaldehyde and formic acid) as end points that can be further electro-oxidized to CO_2, but a fraction of these species is irreversibly lost through diffusion. This loss is minimized in applied systems by recycling the residues, but this procedure takes a toll in terms of the efficiency of the process. The nature of the adsorbed intermediates of methanol electro-oxidation is still under debate, despite some efforts to identify other stable adsorbates[10−12] or reactive intermediates.[13] All possible species obtained from methanol fragmentation have been gathered to form a pictorial mechanism table, but their relative importance in the overall process remains unknown.[14] Fast CO poisoning hampers the investigation of the methanol dehydrogenation steps at low potentials under steady-state conditions in the case of smooth platinum electrodes. Most of the studies of methanol electro-oxidation are made under potentiodynamic conditions,[1−3] and the results are directly applied to the steady-state behavior of the catalysts. As a consequence, the mechanism of methanol dehydrogenation on platinum is still unknown regarding the stable intermediates other than CO and how they couple to each other. This subject is at the very core of the problem when it comes to optimization of the efficiency of methanol electro-oxidation, i.e., favoring the CO_2 pathway.

Platinum nanoparticles are able to electro-oxidize CO at lower overpotentials than smooth platinum. Furthermore, this ability has proven to be dependent on platinum particle size. Not surprisingly, particle size effects have been reported to play a role in the methanol electro-oxidation[15] as well as in the oxidation of its soluble products,[14] formaldehyde and formic acid, when taken as the precursor reactants.

The particle size effect observed on the performance of Pt/C catalysts toward methanol oxidation[15] indicates that the smaller

* To whom correspondence should be addressed. E-mail: nart@iqsc.usp.br.

10.1021/jp063337h CCC: $33.50 © 2006 American Chemical Society
Published on Web 09/06/2006

the average particle size the poorer the electro-catalytic activity for particle sizes in the range below ca. 5 nm. The observed particle size effect on the methanol electro-oxidation is mostly discussed in terms of increasing Pt−CO and Pt−OH bond strength with decreasing particle size.[15−17] This effect seems to be well established. However, to what extent this effect is reflected in the early stages of methanol electro-oxidation is still unclear. This question remains unsolved because the criterion for goodness or badness of a catalyst's performance is based on the inspection of the profile of cyclic voltammograms or other potentiodynamic techniques blind to methanol products partitioning.[14−16,18] Furthermore, previous work regarding the effect of particle size on the methanol oxidation routes either lacks sufficient quantification or suffers from the problem of extrapolation of potentiodynamic results to steady-state systems. In the following pages, differential electrochemical mass spectrometry (DEMS) is used to evaluate the electrocatalytic activity toward methanol oxidation of several carbon supported, highly dispersed platinum particles of different sizes. The influence of particle size distribution in the partitioning of methanol electro-oxidation products is the main focus of the present study. The investigation was conducted under both potentiodynamic and potentiostatic conditions making it possible to discuss how the qualitative results from both regimes compare to each other.

Experimental Section

The working electrodes were prepared by dispersing the catalyst (E-Tek) suspension on a porous carbon cloth and carbon powder assembly. The catalyst powder suspension was prepared by adding 2 mg catalyst to 20 μL Nafion in 5.5 wt % 2-propanol solution. The suspension was sonicated for 10 min. After the complete evaporation of the solvent, some droplets of 2-propanol were added and the coating was spread onto the porous carbon. The electrode was then dried at 80 °C for 1 h. The geometric area of the electrodes was 0.38 cm^2. The mass of the catalysts was constant, and the metal loading ranged from 0.2 to 1.6 mg according to the Pt content in the catalyst.

For the electrochemical and mass spectrometry measurements, a conventional three electrode cell was used at room temperature (25 °C). The counter electrode was a Pt foil, and the standard hydrogen electrode was used as reference. All experiments were carried out in 0.1 M $HClO_4$ solution. Prior to every experiment, the electrode was cleaned in 0.1 M $HClO_4$ by cycling potential between 0.05 and 1.2 V at 50 mV s^{-1} scan rate. Higher potentials were avoided in order to prevent the oxidation of the carbon support. The electrode area was determined by CO oxidative stripping. CO was bubbled for 20 min with the electrode potential held at 0.2 V for CO adsorption at saturation coverage. Argon was then bubbled for over 20 min to remove CO from the solution. The charge of CO oxidative stripping was used to calculate the real area of the catalysts and also used for the normalization and calibration of the DEMS equipment by determining the relation between the faradaic current and the mass signal $m/z = 44$.

DEMS experiments were conducted using a computer controlled quadrupole mass spectrometer, MKS Instruments. Details of the DEMS apparatus and the electrochemical cell assembly can be found elsewhere.[19] Briefly, the method allows the on-line detection of volatile and gaseous products of electrochemical reactions during the application of either a potential scan or a potential step. In a typical DEMS experiment, the current versus potential (time) curves are recorded simultaneously with the mass intensity versus potential (time) curves for selected values of ionic mass-to-charge ratio (m/z).

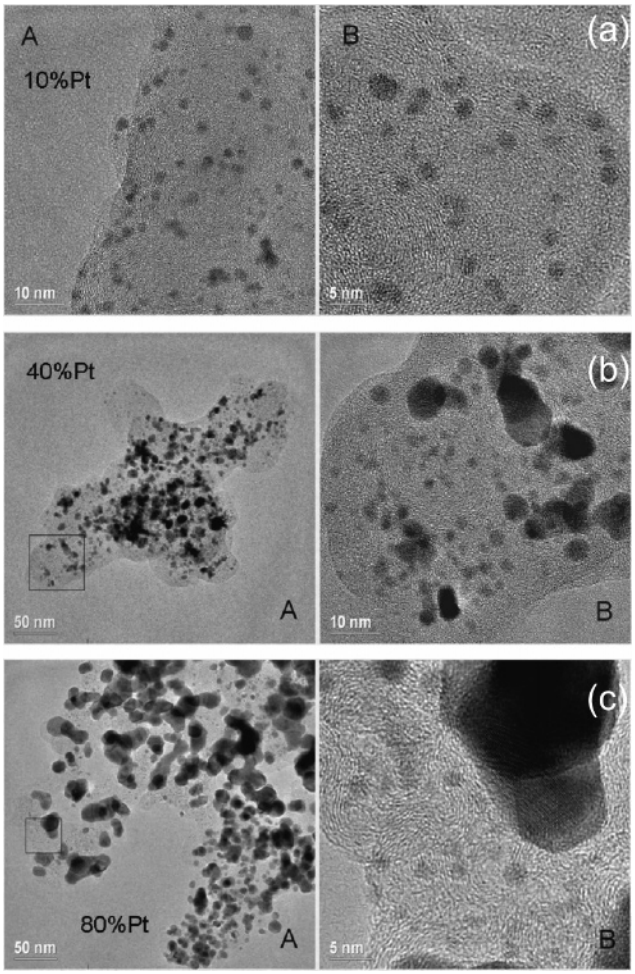

Figure 1. (A) TEM images for the Pt/C X72 Vulcan (E-TEK) catalysts with Pt contents of 10% (a), 40% (b), and 80% (c), respectively. (B) Magnified scale.

Results

Catalyst Characterization. The TEM images for the Pt/C X72 Vulcan with 10%, 40%, and 80% Pt content are presented in Figure 1a−c, respectively. The high crystallinity of the particles could be observed for all catalysts used, as evidenced by examination of Figure 1. The 10% Pt/C catalyst shows a large number of small particles evenly distributed over the carbon support. On the other extremum of the Pt loads used in this study, i.e., the 80% Pt/C particle distribution is not as uniform, showing some degree of agglomeration and the presence of large numbers of small particles (comparable in size to the 10% Pt/C particles) surrounding quite larger particles. This can be better seen in the magnified scale images (labeled B in Figure 1). The morphologies of the remaining Pt/C catalysts studied, namely the 30%, 40%, and 60%, lie between the two extreme cases of 10% and 80%. The histograms of particle size distribution for the complete set of catalysts under examination are presented in Figure 2a−e. The 60% and 80% Pt catalysts comprise significant numbers of particles ranging from 10 to 100 nm sizes, and the respective histograms are presented with different size intervals. The aforementioned presence of constellations of small sized particles is evidenced by the higher frequency of particles below 10 nm in these catalysts. The 80% Pt/C catalyst presents large particles (>10 nm) surrounded by

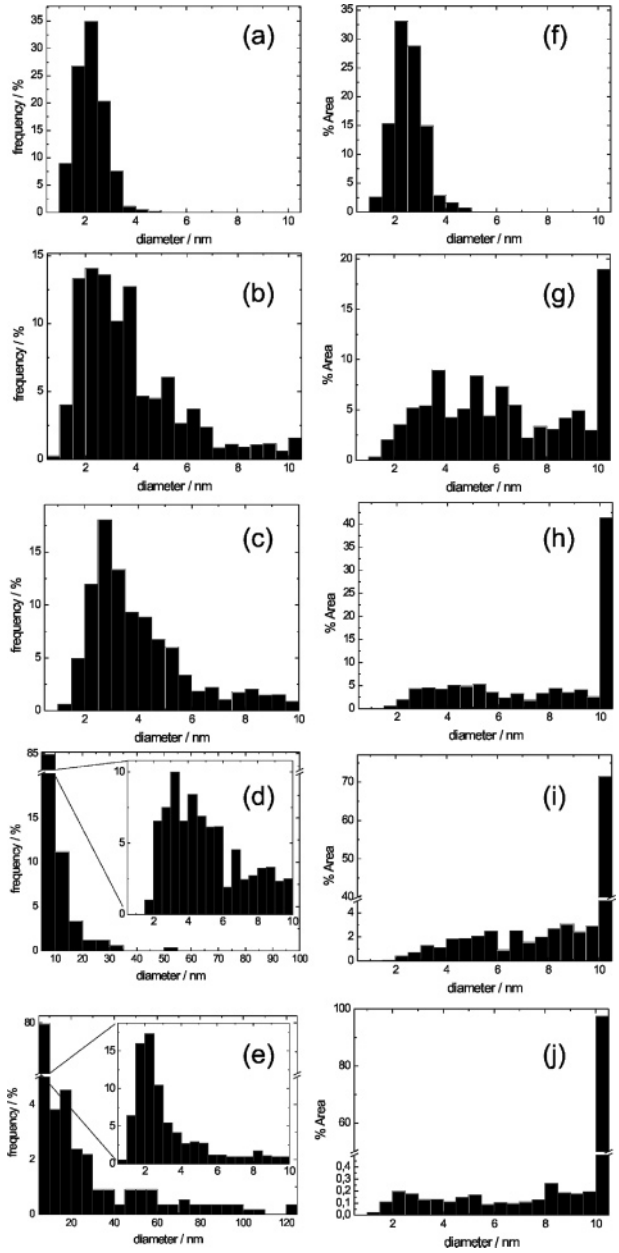

Figure 2. Particle size distribution obtained from the TEM images for the Pt/C X72 Vulcan (E-TEK) catalysts with Pt contents of 10% (a), 30% (b), 40% (c), 60% (d), and 80% (e), respectively. The insets in parts d and e show the size distribution in the 1−10 nm range. (f−j) The relative contribution to the total catalyst area of each size bin of distributions a−e for a cutoff size of 10 nm. Due to the predominant contribution of the larger particles (>10 nm) to the active area of the 60% and 80% catalysts, the axes in parts i and j are broken for a better visualization of the relative contribution of the smaller particles.

small particles with average size sharply centered around 2 nm, and very few particles in the range between 4 and 10 nm (see inset in Figure 2e). In the case of the 60% Pt/C catalyst, on the other hand, the large particles are surrounded by smaller particles with sizes spanning the whole range between 1 and 10 nm, with a significant contribution of particles between 4 and 10 nm in the neighborhood of the large particles.

In general, the catalysts showed very broad spectra of particle sizes with the exception of the sharp distribution of the 10% Pt/C catalyst. This fact makes the concept of mean particle size meaningless for characterizing these catalysts, and the Pt content will be used from now on whenever a comparative graphical representation of any property of these catalysts is necessary.

TABLE 1: Surface Area of the Pt/C Catalysts Used in This Work Estimated from the TEM Images and from the Oxidative Stripping of Adsorbed CO

	area/cm^2		
% Pt/C	TEM	CO stripping	m^2/g Pt TEM
10	225	78.2	113
30	238	126.5	39.7
40	153	106	19.1
60	173	114	14.4
80	62.8	42.0	3.92

Misleading interpretations would arise even if the complete histograms of particle size distribution are considered to describe the electrochemical behavior of these catalysts because, for example, one 10 nm particle is worth 100 1 nm particles in terms of contribution to surface area. From the histograms of Figure 2a−e, the relative contribution to the total surface area was estimated assuming spherically shaped particles. These estimates are presented in Figure 2f−i, using a cutoff size of 10 nm; i.e., the relative contribution to the catalyst surface area from particles larger than 10 nm has all been gathered into the 10 nm size bin in these histograms. This procedure was based on the fact that particle size effects caused by geometrical aspects practically die out for particle sizes above 10 nm irrespective of whether an icosahedron or cuboctahedron shaped model particle is considered.[20−23]

The total Pt surface area of the catalysts was also estimated from the TEM and from the charge of the electrochemical oxidative stripping of 1 monolayer of adsorbed CO.[24] The results are summarized in Table 1. The CO stripping curves for the 10%, 40%, and 80% Pt/C catalysts are presented in Figure 3a. The detailed discussion of the results obtained from the CO stripping experiments is beside the scope of this paper and will be postponed to a forthcoming publication by the authors.

The ratio of the areas estimated from CO stripping and TEM as a function of the %Pt/C contents is presented in Figure 3b. The comparison of the two area estimates is important because the TEM image is a local estimate whereas the CO stripping method provides a global estimation. The agreement between the two methods serves as an evaluation as how representative the TEM images are for describing the catalysts. The surface coverage of a saturated overlayer of CO is about 0.7 for the 40%, 60%, and 80% catalysts, which is in perfect agreement with the values obtained for polycrystalline Pt.[25] For the 30% catalyst, the saturation coverage is about 0.55, and for the 10% catalyst, only about 0.35 or half the expected value. One possible explanation for the surface area discrepancies as estimated by TEM and electrochemical stripping in the cases of the 30% and 10% catalysts is the observation is that some of the Pt particles are not electrochemically active because they are not accessible to the electrolyte.[26] In agreement with the data of Table 1, Ticianelli et al.[26] found the area of Etek Pt/C gas diffusion electrodes estimated by hydrogen upd to be smaller than that estimated from TEM, by a factor of 2.5 for the 10% Pt/C and 1.5 for the 20% and 40% Pt/C catalyst. This discrepancy in area estimation was also observed for the thin porous coating electrode assembly.[27,26] In the latter configuration, where no Nafion impregnation was carried out, the area estimated by hydrogen upd was about 50% for the 10%, 20%, 30%, 40%, 60%, and 80% Pt/C catalysts. Mcbreen and Mukerjee[17,23] suggested that small Pt particles might undergo deformation at potentials in the hydrogen region from XANES XSAFS data, but the extent to which this affects area estimation by hydrogen is unknown. Jusys et al.[5,6] found no discrepancies between the two methods (electrochemical−CO/H_{upd} stripping−and TEM)

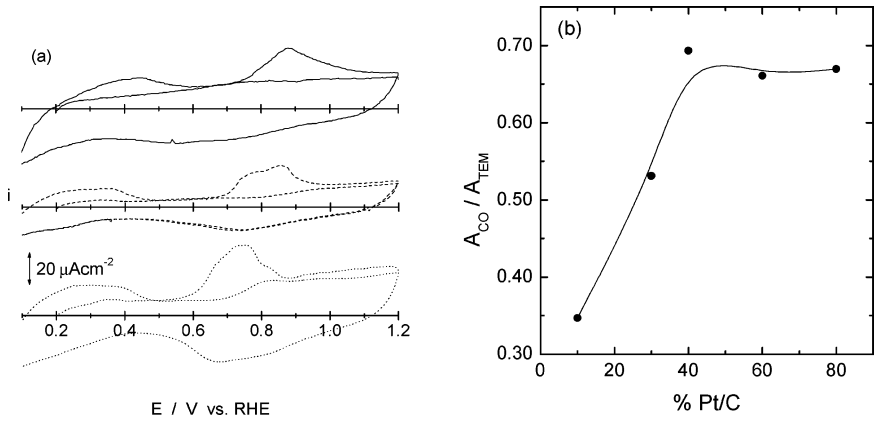

Figure 3. (a) CO electrooxidative stripping curves for the 10% (—), 40% (---), and 80% (···) Pt/C catalysts at 10 mV s^{-1}. (b) Ratio of the areas estimated from CO stripping and TEM as a function of the Pt contents in the Pt/C catalysts.

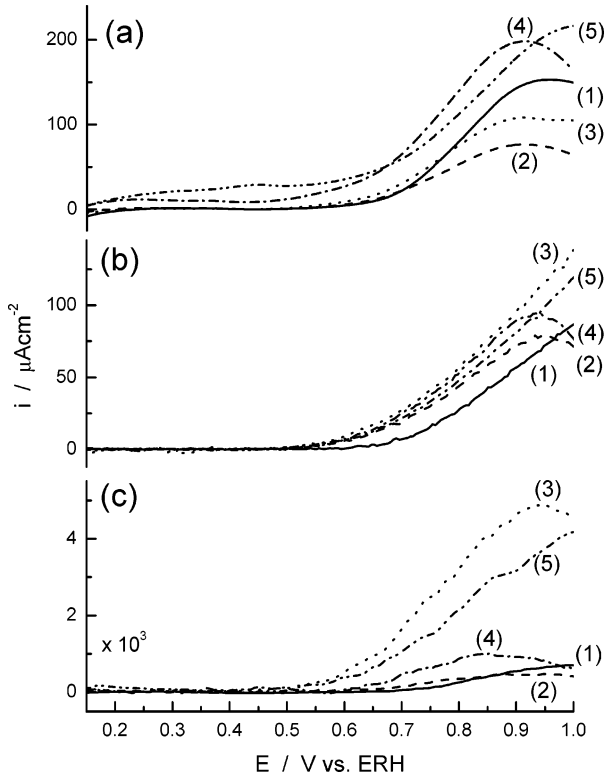

Figure 4. Voltammetric curves for methanol electro-oxidation in 0.1 M $HClO_4$ + 0.1 M Me-OH: overall faradaic current density (a), CO_2 route current density from m/z = 44 (b), and normalized m/z = 60 signal (c). 10% Pt/C (—, 1), 30% Pt/C (---, 2), 40% Pt/C (···, 3), 60% Pt/C (-·-·, 4), and 80% Pt/C (-··-··, 5). Scan rate = 10 mV s^{-1}.

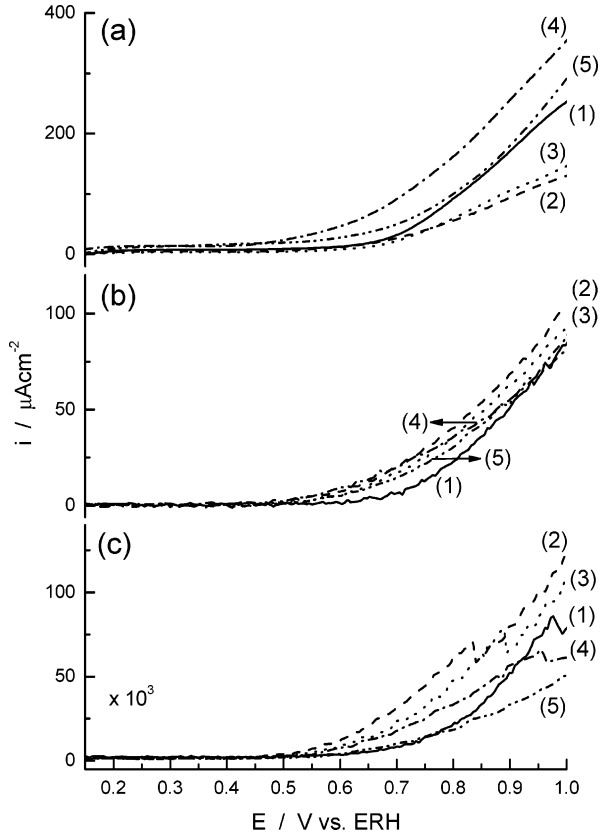

Figure 5. Voltammetric curves for methanol electro-oxidation in 0.1 M $HClO_4$ + 2.0 M Me-OH: overall faradaic current density (a), CO_2 route current density from m/z = 44 (b), and normalized m/z = 60 signal (c). 10% Pt/C (—, 1), 30% Pt/C (---, 2), 40% Pt/C (···, 3), 60% Pt/C (-·-·, 4), and 80% Pt/C (-··-··, 5). Scan rate = 10 mV s^{-1}.

of area estimation in a ultrathin film Pt/C electrode configuration. This indicates that the differences are very likely to come from structural factors such as particle wetting, porous blockage, etc., which are dependent on electrode preparation, as pointed out in ref 26.

Potentiodynamic Methanol Oxidation. The voltammetric curves for methanol oxidation of the supported nanoparticle electrodes are presented in Figures 4 and 5 for methanol concentrations of 0.1 and 2 M, respectively. The faradaic current (Figures 4 and 5a), as well as the mass intensities at m/z 44 (Figures 4 and 5b) and m/z 60 (Figures 4 and 5c) in these figures are normalized to their respective counterparts of faradaic current and m/z 44 signal intensity in the CO stripping experiments.

The highest faradaic current density is observed for the 60% Pt/C catalyst, with decreasing values for the 80%, 10%, 40%, and 30% Pt/C catalysts, in this order. In the case of the 0.1 M MeOH solution, this trend is observed up to about 0.85 V, just before the maximum of the current density peak is observed. The appearance of this peak is certainly related to methanol diffusion problems as it is not observed in the case of the more concentrated solution. Furthermore, in the case of the 0.1 M solution, the differences in current density are more clearly observed, whereas for the 2.0 M solution the values of current density observed for the 10% and 80% Pt/C are very close to each other as are the values for the 30% and 40% catalysts. The contribution of the CO_2 formation route to the overall current density is roughly similar for all catalysts irrespective of the methanol concentration, as can be observed in Figures 4b and 5b. An exception to this general behavior is observed for the 10% Pt/C catalyst, in which case the onset of the CO_2

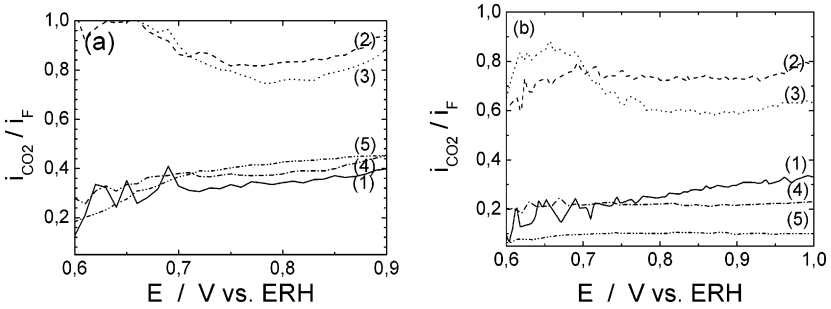

Figure 6. Fraction of overall current density of methanol electro-oxidation in 0.1 M (a) and 2.0 M (b) MeOH from the CO_2 route. 10% Pt/C (—, 1), 30% Pt/C (---, 2), 40% Pt/C (···, 3), 60% Pt/C (-·-·, 4), and 80% Pt/C (-···-··, 5). Scan rate = 10 mV s^{-1}.

formation is shifted about 50 mV to more positive potentials compared with the other catalysts. In a detailed analysis, the differences in the mass signals of the catalysts are discussed separately for each concentration. The two data sets obtained at different methanol concentrations cannot be directly compared when discussing the $m/z = 60$ signal used to track the formic acid formation. This is because the $m/z = 60$ signal is due to the main fragment of methylformate formed via

$$H_3COH + HCOOH \leftrightarrow HCOOCH_3 + H_2O \qquad (1)$$

Thus, the methylformate signal depends on the concentrations of both formic acid and methanol. This explains the difference, in an order of magnitude sense, in the $m/z = 60$ signal for the two methanol concentrations.

In 0.1 M methanol solution, the maximum current density due to the CO_2 route is observed for the 40% Pt/C catalyst, followed by the 60%, 80%, 30%, and 10% Pt/ C catalysts, in this order, as shown in Figure 4b. A similar trend is observed for the formic acid signals of Figure 4c, except for the case of the 60% Pt/C which produces a lower amount of formic acid than the 80% catalyst. Both the route that leads to CO_2 and the route that leads to formic acid require the formation of oxygenated species. The observed similarity in the trends of CO_2 and formic acid production may be regarded as a reflection of the ability of the catalysts to produce oxygenated species. However, oxygenated species formation is not the only determining factor in the methanol oxidation process; notably, the differences in the $m/z = 60$ signal among the catalysts are greater than the differences in the CO_2 signal. This fact indicates that the differences in the particle sizes and size distributions of the catalysts have a substantial effect in the early stages of methanol dehydrogenation. This effect is made more evident when the performance of the catalysts is compared pairwise: the 40% Pt/C produced the largest CO_2 and formic acid outputs whereas its faradaic current density is nearly half of that of the 80% catalyst, thus, the difference in faradaic current density is likely the result of a much larger contribution from the route leading to formaldehyde. The same reasoning applies to the 10% and 60% catalysts. Under potentiodynamic conditions there may be some contribution to the excess current from the accumulation of adsorbed intermediates other than formaldehyde. However, as will be seen further on, the same trend is observed under potentiostatic conditions, providing strong evidence that the primary contributor to the excess current is indeed the formaldehyde production. The ratio of the current density from the CO_2 route to the overall faradaic current density for the 0.1 M methanol solution is presented in Figure 6a.

The 30% Pt/C catalyst showed the best selectivity toward the CO_2 route with about 90% on average of the faradaic current coming from this process. The 40% Pt/C catalyst also exhibited a remarkable performance with an 80% efficiency on average, whereas the 10%, 60%, and 80% Pt/C catalysts are poor CO_2 producers. The behavior of the 40% Pt/C catalyst allows for a rough estimation of the extent of the contribution of the formic acid route to the overall faradaic current measured. The 40% catalyst is responsible for the largest formic acid signal, which accounts for at most 20% of the overall faradaic current, (assuming no formaldehyde is being produced). Thus, the largest formic acid signal would account for only about 20 μA cm^{-2}. This is a very rough estimation but serves as an upper bound for the contribution of the formic acid route to the faradaic current density. As the remaining catalysts (10%, 60%, and 80%) showed much lower formic acid signals but higher overall faradaic currents, it must be that formaldehyde is the main product of methanol oxidation for the 10%, 60%, and 80% Pt/C catalysts. The formaldehyde production does not involve the formation of adsorbed oxygenated species, and thus, it reinforces the view that the influence of particle morphology cannot be fully explained by the commonly held idea that different electrocatalytic activity is based only on differing abilities to adsorb oxygenated species. The particle morphology seems to play a key role in determining the intermediate stages of methanol dehydrogenation.

In 2.0 M methanol solution, the same considerations can be made as before. The ratio of the current density from the CO_2 route to the overall faradaic current density for the 2.0 M methanol solution is presented in Figure 6b. The selectivity of the catalysts toward the CO_2 route showed the same trend as before, except that quantitatively the selectivity is somewhat smaller for the higher methanol concentration. It is interesting to notice that the highest CO_2 producing catalysts, 30% and 40% Pt/C, showed very similar faradaic and CO_2 current density for both methanol concentrations. The weak dependence of the current density on the methanol concentration has been observed earlier.[14,29] This indicates that the methanol adsorption is not rate determining in this process. Considering that the 30% Pt/C catalyst presents the highest CO_2 and formic acid outputs and the lowest faradaic current density, it again seems that the higher current densities observed for the 10%, 60%, and 80% Pt/C catalysts in 2.0 M methanol solution are due to formaldehyde production. Notably, the faradaic currents observed for the 30% catalyst in 0.1 and 2.0 M MeOH are roughly equal, whereas the faradaic currents observed for the 10%, 60%, and 80% catalysts vary by almost 100% with concentration. This implies that methanol concentration exerts the strongest effect on formaldehyde producing catalyst. The comparison of the formic acid output for the two methanol concentration is not straightforward as pointed out earlier, but the similarities in the faradaic and CO_2 outputs for the 30% Pt/C catalyst in 0.1 and 2.0 M (one can take the 40% example as well) suggest that the differences observed for these two concentrations in the $m/z =$

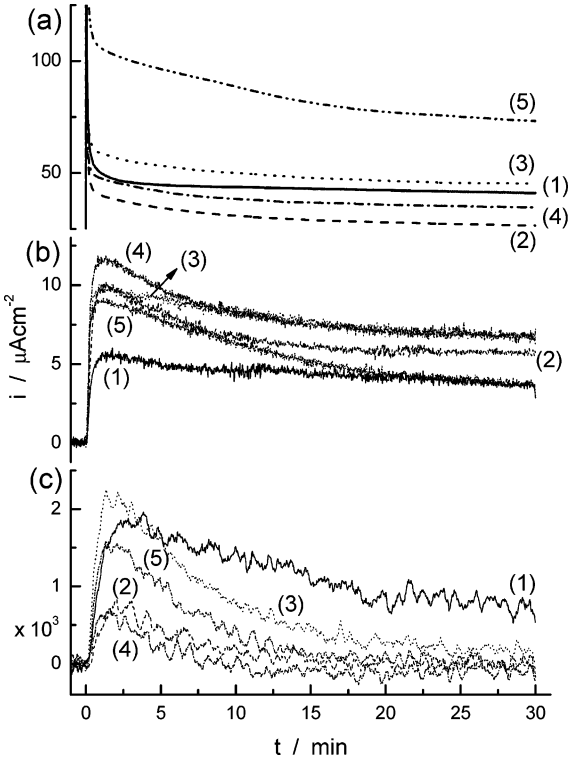

Figure 7. Chronoamperometric curves for methanol electro-oxidation in 0.1 M $HClO_4$ + 0.1 M MeOH: overall faradaic current density (a), CO_2 route current density from $m/z = 44$ (b), and normalized $m/z = 60$ signal (c). 10% Pt/C (—, 1), 30% Pt/C (---, 2), 40% Pt/C (•••, 3), 60% Pt/C (-•-•, 4), and 80% Pt/C (-•••-••, 5). $E = 0.7$ V vs RHE.

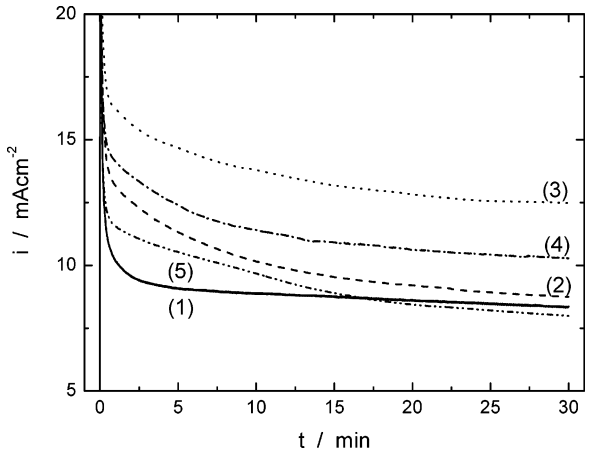

Figure 8. Same as Figure 7a, normalized by the geometric electrode area. 10% Pt/C (—, 1), 30% Pt/C (---, 2), 40% Pt/C (•••, 3), 60% Pt/C (-•-•, 4), and 80% Pt/C (-•••-••, 5). $E = 0.7$ V vs RHE.

60 signal are solely due to the methanol concentration influence via eq 1 and not to any intrinsic catalytic effect.

Steady-State Methanol Oxidation. In fuel cell applications the stability of the catalyst under the reaction conditions is important. Chronoamperometric curves generally can give clues about catalyst poisoning or stability loss. The main goal here is not to check the long-term operation and stability of the catalyst, but to check if there is a rapid poisoning of the catalyst upon methanol oxidation. The chronoamperometric data reported in Figures 7−9 were obtained for methanol oxidation at 0.7 V. Although this is already too positive a potential for an efficient fuel cell, data from this potential are valid for the purposes of the present study, the evaluation of the CO_2 selectivity as a function of the particle size and morphology and the possible poisoning of the catalyst.

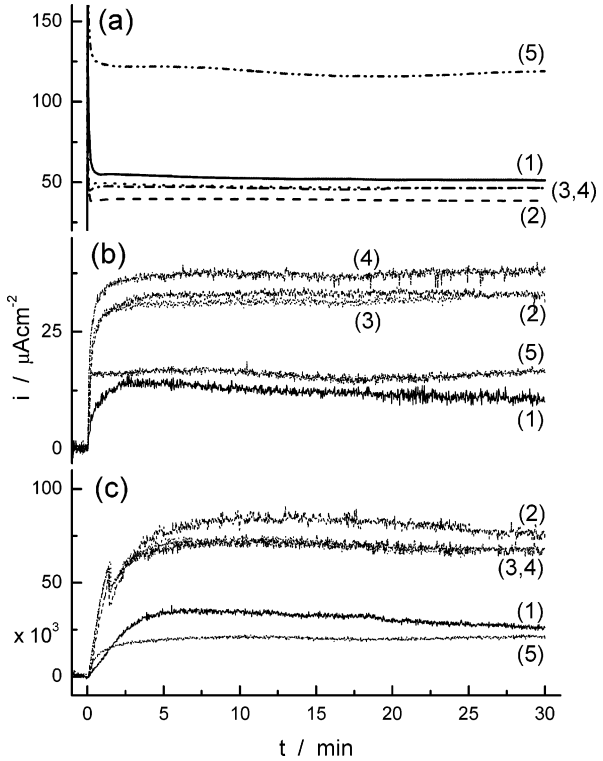

Figure 9. Chronoamperometric curves for methanol electro-oxidation in 0.1 M $HClO_4$ + 2.0 M Me-OH: overall faradaic current density (a), CO_2 route current density from $m/z = 44$, (b) and normalized $m/z = 60$ signal (c). 10% Pt/C (—, 1), 30% Pt/C (---, 2), 40% Pt/C (•••, 3), 60% Pt/C (-•-•, 4) and 80% Pt/C (-•••-••, 5). $E = 0.7$ V vs RHE.

It can be seen in Figure 7 that for a methanol concentration of 0.1 M the normalized current decreases with time, probably due to diffusion effects. Note that the current drop with time is dramatic for the $m/z = 60$ mass signal, practically vanishing for all catalysts. The reason is that the methylformate concentration decreases as the bulk methanol concentration decreases, the only exception being the 10 % Pt/C catalyst for which the $m/z = 60$ signal decays more slowly as does the faradaic and CO_2 current density.

At this point it is important to consider the diffusion effects on the methanol concentration near the electrode. The diffusive flux of methanol in solution is determined by the geometrical area of the electrode; that is, the geometrical area is the limiting factor for methanol diffusion from the solution. The current density data in terms of electrode geometrical area (0.38 cm^2) are presented in Figure 8 for the case of the 0.1 M methanol solution. As can be seen, the current densities range from 10 to 15 mA cm^{-2}. If it is assumed that a steady methanol concentration profile in solution has been achieved, one can roughly estimate the methanol concentration drop at the solution/catalyst interface by

$$\Delta C = \frac{i_f \delta_N}{\langle z \rangle FD} \tag{2}$$

where the i_f, δ_N, $\langle z \rangle$, F, D are the faradaic current density, the Nernst diffusion layer thickness, the average number of electrons transferred by methanol molecule, the Faraday constant and the diffusion coefficient of methanol, respectively. Using a value of 10^{-5} cm^2 s^{-1} for the diffusion coefficient, 5×10^{-2} cm for the diffusion layer thickness due to natural convection in a quiescent solution and a proper $\langle z \rangle$ according to the CO_2 efficiency, it follows that, on average, the methanol concentra-

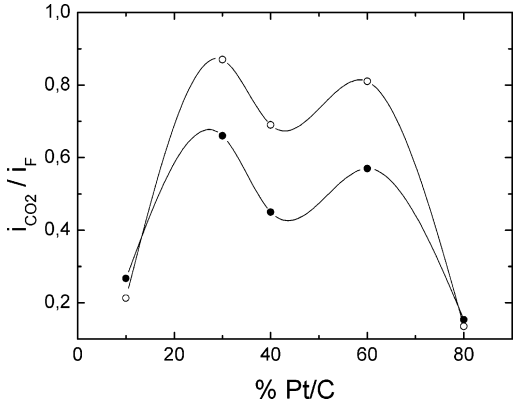

Figure 10. Fraction of overall current density of methanol electro-oxidation from the CO_2 route in 0.1 M (-●-) and 2.0 M (-○-) MeOH as determined under steady conditions. $E = 0.7$ V vs RHE.

tion drop at the solution interface is close to 0.1 M. It means that in the case of the 0.1 M solution, the electro-oxidation process is very close to being diffusion limited. This is confirmed by the fact that the $m/z = 60$ signal practically dies out while the faradaic and CO_2 current densities remain finite and measurable. The lack of $m/z = 60$ signal causes complete loss of information on the relative importance of the contribution of the formic acid route. Furthermore, approaching the diffusion limiting situation poses a problem in defining the current density of a porous electrode in terms of real catalyst area because in a diffusion limited situation, the innermost particles of the electrode suffer from methanol starvation and are thus electrochemically inactive for steps involving the methanol species. As such, the detailed analysis of data of Figure 7 is skipped. Despite the difficulty in normalizing the current, the assessment of the efficiency of the CO_2 route is not disturbed as the normalization factors cancel out. The ratio of the current density from the CO_2 route to the overall faradaic current density for the 0.1 M methanol solution is presented in the solid curve of Figure 10.

The decrease in current and mass signal for the 2.0 M methanol concentration is not as pronounced, since diffusion effects are not critical in this case. This can be confirmed by the fact that the faradaic current densities are of the same order of magnitude for both methanol concentrations (compare Figures 7a and 9a). Thus, for the 2.0 M methanol solution the concentration at the electrode/solution interface is disturbed by at most 5%.

As can be seen in Figure 9, the 30%, 40%, and 60% Pt/C catalysts exhibit a similar behavior in the faradaic and CO_2 current densities and formic acid yield as well. These catalysts also present a higher selectivity toward the CO_2 electro-oxidation route as shown in Figure 10, curve formed with open circles. The high selectivity of the 30% and 40% Pt/C catalyst has been inferred from the potentiodynamic experiments. However, the outstanding performance of the 60% Pt/C catalyst (even better in CO_2 yield than the 40% catalyst) under steady-state conditions is a surprising outcome considering the poor performance under potentiodynamic conditions (see Figure 6). This indicates that one should be careful judging catalyst performance from potentiodynamic experiments. The poor performance of the 10% and 80% Pt/C catalysts follows the same trend as in the previous case. Accordingly, it seems that the same reason underlies the poor performance, i.e., the high yield in formaldehyde. From Figure 9 it can be seen that the 10% Pt/C provides about half the yield in CO_2 and formic acid with respect to the 30%, 40%, and 60% catalysts, but it presents a higher overall faradaic current density. This undesired selectivity toward formaldehyde formation is even more pronounced in the case of the 80% Pt/C catalyst.

Discussion

Before discussing the differences in electrocatalytic activity observed among the catalysts investigated, it is worthwhile to discuss the similarities in their behavior that would allow for elucidation of some generalizations regarding the process of methanol electro-oxidation. One important observation is the fact that the values of the faradaic current density in Figures 4 and 5 do not reflect the large difference in methanol concentration utilized to obtain the two sets of data. The lack of variation of faradaic current with methanol concentration is even more striking when the steady-state data from Figures 7 and 9 are considered. The comparable current densities observed for the 2.0 M methanol solution and the 0.1 M methanol solution, for which the methanol concentration at the interface is very low, mean that the methanol concentration is not determinining the kinetics of the overall reaction. This indicates that the earlier stages of methanol adsorption and dehydrogenation are not rate-determining steps. Indeed, Kauranen et al.[29] have found that the reaction order for the methanol electro-oxidation on 40% Pt/C gas diffusion electrodes is practically zero for methanol concentrations above 0.5 M. The CO_2 production current is quite similar for both methanol concentrations in the case of Figures 4 and 5. These observations strongly suggest that the reaction of the methanol dehydrogenation products with oxygenated species is the rate-determining step at the considered potential.

The results presented in this work clearly show the strong dependence of the catalytic activity of the Pt/C catalysts on particle size. If one considers only the faradaic current density, one would be led to the misapprehension that the specific activity decreases with decreasing average particle size, as is implied by inspection of the data in Figures 4, 5, 7, and 9, in agreement with the reported data in the literature.[14−16] The perceived dependence of activity on particle size led these authors to ascribe the differences in specific catalytic activity to the higher binding energy of the oxygenated species on lower coordination sites,[15,17,23] which are more abundant in smaller particles. Other authors explained the activity dependence on the basis of lower concentrations of contiguous Pt surface sites of high coordination number (ensembles) on the smaller particles.[14,16] Both of these explanations are morphologic in nature and would lead to a monotonic increase in the electrocatalytic activity with increasing particle size, since edge concentrations and terrace sizes change monotonically with particle diameter. It must be noticed that this analysis is based on ideally geometrical particles with integral numbers of shells. This monotonic variation in the edge concentrations and terrace sizes with particle size is disturbed if incomplete shells are also considered.[22] However, in favor of this analysis one could claim the fact that this approach led Kinoshita[21] to a very good correlation between the outcome of this analysis and experimental data of electroactivity of Pt/C catalysts toward oxygen reduction reaction. If one assumes a monotonic increase in electrocatalytic activity with particle size, then one expects that the optimum mass activity would be observed on catalysts which have a balance of high activity and high area-to-mass ratio. However, when efficiency in terms of electrons produced per methanol molecule is considered, a different picture emerges. As can be seen in Figures 6 and 10, the efficiency in CO_2 production shows a maximum for the 30%, 40%, and 60% Pt/C catalysts (the maximum at 60% being observed in the case of

the potentiostatic experiments only) which present intermediate particle sizes.

Also remarkable about the partitioning of the electro-oxidation products for the considered catalysts is the fact that the formic acid yield does not exceed 10−20% in terms of contribution to overall faradaic current density. Furthermore, the contribution of formic acid to the overall faradaic current is proportional to the CO_2 yield. In agreement with this observation, on 20% Pt/C catalysts with low electrode platinum loading (2 μg platinum), the formic acid contribution to the faradaic current is less than 10% while the CO_2 contribution is approximately 30%.[5] This has the important consequence that the loss in the CO_2 production efficiency is strictly related to the increase in formaldehyde production. Indeed, literature data show that the formaldehyde yield is higher than CO_2 for low platinum loading.[6] Moreover, an increase of CO_2 yield upon increasing the platinum loading is obtained at the expense of a formaldehyde yield decrease.[5]

As mentioned in the Results section, with the exception of the 10% Pt/C catalyst, the broad particle size distribution makes the concept of average particle size of little use in order to understand the catalyst behavior. The behavior of the 10% Pt/C catalyst, with the sharper distribution of the particles around 2.5 nm (see Figure 2a,f), can be understood in terms of the concepts of ensemble effects and Pt−O binding on lower coordination sites. In fact, as can be observed in Figures 4 and 5, the onset potential for the formation of CO_2 and formic acid is shifted toward the more positive potential region, in accordance with the concept of higher binding energy intermediates for small particles. This explanation is in perfect agreement with the higher potentials required for the oxidative stripping of one monolayer of adsorbed CO[30,31] (refer to Figure 3a). The larger amounts of formaldehyde produced can be understood in terms of either ensemble effects or in terms of repulsive forces felt by the adsorbed formaldehyde due to higher coverage of a more strongly bonded intermediate.[5] However, any attempt to use the same concepts to explain the behavior of the 80% Pt/C catalyst fails miserably. This catalyst produces the largest amount of formaldehyde in the investigated set whereas the contribution to the catalyst area comes almost entirely from particles larger than 10 nm, despite the large number of smaller particles. This result was quite unexpected and cannot be accounted for by either the ensemble concept or the repulsive effect concept, as this catalyst showed the lowest peak potential for the oxidative CO stripping (Figure 3a). Savinova et al.[30] have pointed that the CO stripping experiments cannot be explained only in terms of particle morphology, but an intrinsic effect of particle sizes must also be considered. If this is so, it would be plausible that larger particles present intrinsically lower binding energies for adsorbed intermediates. If one considers that the adsorption energy of the adsorbed formaldehyde formed in the early stage of methanol dehydrogenation is smaller on larger particles, then desorption of this intermediate to the solution would be more facile, and this would provide the observed drain of formaldehyde to the solution.

The 30% and 40% Pt/C catalysts demonstrated high efficiency in CO_2 yield and very low or insignificant formaldehyde yield under both potentiostatic and potentiodynamic conditions. These catalysts present a reasonably large contribution in area from particles in the size range 3−9 nm. This would imply that the optimum particle size for the complete methanol electro-oxidation lies in this range. The contribution of the particles with sizes in the same range as those in the 10% Pt/C catalyst can be neglected in this qualitative analysis, as can be seen in Figure 2g,h. However, 20−40% of the 30% and 40% catalysts' surface areas come from larger particles just like those found in the 80% Pt/C catalyst. That is, 30% and 40% catalysts would have partial 80% Pt/C "character". The fact that the 80% catalyst and the 30% (or 40%) catalysts have some morphological similarity but very dissimilar electrocatalytic activities can be rationalized if we consider the fact that the larger particles in the 30% and 40% catalysts are always surrounded by a large number of medium sized particles (not the case for the 80% catalyst where the relative contribution of large particles is much greater than the contribution from the smaller particles). It would then be possible that in the case of the 30% and 40% Pt/C, the formaldehyde formed on the large particles is further oxidized (very efficiently) by the neighboring smaller particles. In this way, the large particles keep the smaller particles fed for the formaldehyde oxidation in a sort of bifunctional mechanism. Even if the 80% Pt/C presents a large number of smaller particles, it seems that the poor contribution in terms of area from these smaller particles hinders the further oxidation of formaldehyde in a significant way, as this latter species is produced in greater amounts than the small particles can handle.

The nearest neighbor distances between particles in all the catalysts are on the order of tens of nanometers (see Figure 1) which makes it quite plausible for the larger and smaller particles to be coupled by formaldehyde diffusion. This hypothesis is very attractive to explain the discrepancies between the potentiostatic and potentiodynamic behavior of the 60% Pt/C catalyst. In this case, the contribution of particles larger than 10 nm to the area of this catalyst is about 70%. Under potentiodynamic conditions the transient nature of the diffusion profile would hinder the optimum interparticle formaldehyde exchange. It is worthwhile to note that the voltammetric curves for the 60% and 80% Pt/C catalysts show higher faradaic current densities with respect to the remaining catalysts at potentials lower than 0.6 V. This is easily explained by the fact that formaldehyde formation does not require the presence of any adsorbed oxygenated species, in harmony with the discussion above.

The concept of the coupling of small and larger particles over distances on the order of nanometers in a bifunctional mechanism effectively explains the data presented in this paper and is quite novel in the field of dispersed catalysts. Jusys et al.[6] have used the concept of trapping of formaldehyde inside the pores of the gas diffusion electrode which would provide the retention time necessary for the formaldehyde to be further oxidized at locations far from where it has been formed. These authors explored this phenomenon to account for the increase in the CO_2 yield upon increasing the Pt loading of Pt/C electrodes. They have found that the CO_2 yield changed from 30% to 80% for platinum loadings ranging from 7 to 35 μg cm^{-2}. Despite the fact that diffusion is responsible for the coupling in the mechanism suggested in this paper and in the mechanism proposed by Jusys et al.,[6] the two mechanisms differ in that the distance scales in which the two phenomena operate are vastly different. In the case discussed in this paper, the phenomenon occurs in the nanometer range, more like a bifunctional mechanism as discussed in alloys or modified smooth electrodes. This fact makes it insensitive to the thickness of the electrode (in the microns range). In contrast, the mechanism of Jusys et al.[6] is one of long range coupling, inherently sensitive to layer thickness.

As a last comment, the trapping of soluble intermediates seems to play a decisive role in the product partitioning for the methanol electro-oxidation on Pt/C catalysts, and should occur in addition to the phenomenon suggested here. However, the

TABLE 2: Tap Density of the Pt/C Catalysts Used in This Work Obtained from the Vendor's Website

% Pt/C	TAP density/g cm^{-3}
10	0.225
30	0.304
40	0.346
60	0.445
80	0.590

concept of trapping alone cannot explain the results obtained (Figure 10). In Table 2 the tap densities of the Pt/C catalysts used in this work are presented. Assuming that, for fixed catalyst mass, the thickness of the catalytic layers would roughly follow the reciprocal of the tap densities in Table 2, it follows that some inconsistencies arise when one tries to use the concept of byproduct trapping to explain the data of Figure 10. Specifically, the differences in the activity and selectivity of the 40%, 60%, and 80% Pt/C catalysts, when compared pairwise, are impossible to explain in light of the data presented in Table 2. The 40% and 60% catalysts barely differ in their product distribution and efficiency whereas they differ in layer thickness by about 30%. The estimated difference in thickness between the 60% and 80% catalysts is also about 30%, but the difference in their efficiencies is remarkable.

Conclusion

The efficiency of electro-oxidation of methanol on supported platinum nanoparticles shows a strong dependence on particle size distribution. For us to understand the particle size effects on the electrocatalytic activity, not only the morphology, but also the coupling in the nanometer range among particles of different sizes via soluble products must be considered in order to gain a better insight into the overall effect.

For catalysts presenting only small particles (less than 10 nm), there is an optimum particle size range for efficiently electro-oxidizing methanol to CO_2 between 3 and 10 nm. Loss in efficiency was observed for either too small or too large particles leading mainly to the partial oxidation of methanol to formaldehyde. In the case of overly small particles, the loss in efficiency can be accounted for by morphological considerations, whereas in the case of overly large particles (>10 nm) the more facile formaldehyde desorption to the solution becomes critical.

In the case of catalysts comprising particles with a large discrepancy in size, and consequently in activities toward methanol/formaldehyde dehydrogenation, the following picture arises: whenever particles with different sizes are close enough to be coupled through diffusion without significant loss (in the nanometer range), they exchange soluble products in the form of a bifunctional mechanism. This concept was used in order to explain the enhanced activity observed for the 60% Pt/C catalyst.

Acknowledgment. The authors would like to thank the Brazilian funding agencies FAPESP, CAPES, and CNPq for financial support. The authors are also grateful to the LME/LNLS for technical support during the electron microscopy work.

References and Notes

(1) Jarvi, T. D.; Stuve, E. M. In *Electrocatalysis*; Lipkowski, J., Ross, P. N., A., Eds.; Wiley-VCH: Heidelberg, 1998; p 75.
(2) Hamnett, A. In *Interfacial Electrochemistry*; Wieckowski, A., Ed.; Marcel Dekker: New York, 1999;.p 843.
(3) Iwasita, T. *Electrochim. Acta* **2002**, *47*, 3663.
(4) Iwasita, T.; Vielstich, W. *J. Electroanal. Chem*. **1986**, *201*, 403.
(5) Jusys, Z.; Behm, R. J. *J. Phys. Chem.* B **2001**, *105*, 10874.
(6) Jusys, Z.; Kaiser, J.; Behm, R. J. W. *Langmuir* **2003**, *19*, 6759.
(7) Wasmus, S, Wang, J. T.; Savinell, R. F. *J. Electrochem. Soc*. **1995**, *142*, 3825.
(8) Spendelow, J. S.; Wieckowski, A. *Phys. Chem. Chem. Phys*. **2004**, *6*, 5094.
(9) Antolini, E. *Mater. Chem. Phys.* **2003**, *78*, 563.
(10) Khazova, O. A.; Vasilev, Y. B.; Bagotski, V. S. *Int. Chem. Eng*. **1966**, *6*, 24.
(11) (a) Wilhelm, S.; Iwasita, T.; Vielstich, W. *J. Electroanal. Chem*. **1987**, *238*, 283. (b) Iwasita, T.; Vielstich, W.; Santos E. *J. Electroanal. Chem*. **1987**, *229*, 367.
(12) Iwasita, T.; Nart, F. C. *J. Electroanal. Chem*. **1991**, *317*, 291.
(13) Jarvi, T. D.; Sriramulu, S.; Stuve, E. M. *Colloids Surf., A* **1998**, *134*, 145.
(14) Park, S.; Xie, Y.; Weaver, M. J. *Langmuir* **2002**, *18*, 5792.
(15) Frelink, T.; Visscher, W.; van Veen, J. A. R. *J. Electroanal. Chem*. **1995**, *382*, 65.
(16) Park, S.; Tong, Y.; Wieckowski, A.; Weaver, M. J. *Langmuir* **2002**, *18*, 3233.
(17) Mukerjee, S.; McBreen, J. *J. Electroanal. Chem*. **1998**, *448*, 163.
(18) Glouaguen, F.; Léger, J. M.; Lamy, C. *J. Appl. Electrochem*. **1997**, *27*, 1052.
(19) de Souza, J. P. I.; Queiroz, S. L.; Nart, F. C. *Quím. Nova* **2000**, *23*, 384.
(20) Kinoshita, K. In *Modern Aspects of Electrochemistry*; Bockris, J. O'M., Conway, B. E., White, R. E., Eds.; Plenum Press: New York, 1982; Vol. 14, p 557.
(21) Kinoshita, K. *J. Electrochem. Soc*. **1990**, *137*, 845.
(22) Benfield, R. E. *J. Chem. Soc., Faraday Trans*. **1992**, *88*, 1107.
(23) McBreen, J.; Mukerjee, S. In *Interfacial Electrochemistry*; Wieckowski, A., Ed.; Marcel Dekker: New York, 1999; p 895.
(24) Iúdice de Souza, J. P.; Iwasita, T.; Nart, F. C.; Vielstich, W. *J. Appl. Electrochem*. **2000**, *30*, 43.
(25) Biegler, T.; Rand, D. A. J.; Woods, R. J. *J. Electroanal. Chem*. **1971**, *29*, 269.
(26) Ticianelli, E. A.; Berry, J. G.; Srinivasan, S. *J. Appl. Electrochem*. **1991**, *21*, 597.
(27) Perez, J.; Gonzalez, E. R.; Ticianelli, E. A. *Electrochim. Acta* **1998**, *44*, 1329.
(28) Calegaro, M. L.; Perez, J.; Tanaka, A. A.; Ticianelli, E. A.; Gonzalez, E. R. *Denki Kagaku* **1996**, *64*, 436.
(29) Kauranen, P. S.; Skou, E.; Munk, J. *J. Electroanal. Chem*. **1996**, *404*, 1.
(30) Maillard, F.; Savinova, E. R.; Simonov, P. A.; Zaikovskii, V. I.; Stimming, U. *J. Phys. Chem. B* **2004**, *108*, 17893.
(31) Arenz, M.; Mayrhofer, K. J. J.; Stamenkovic, V.; Blizanac, B. B.; Tomoyuki, T.; Ross, P. N.; Markovic, N. M. *J. Am. Chem. Soc.* **2005**, *127*, 6819.